Sensors and Actuators B 235 (2016) 525–534

Contents lists available at ScienceDirect

Sensors and Actuators B: Chemical

journal homepage: www.elsevier.com/locate/snb

Chemoresistive micromachined gas sensors based on functionalized metal oxide nanowires: Performance and reliability

S. Vallejos[a,*], I. Grácia[b], O. Chmela[a], E. Figueras[b], J. Hubálek[a], C. Cané[b]

[a] SIX Research Centre, Faculty of Electrical Engineering and Communications, Brno University of Technology, 601 90 Brno, Czech Republic
[b] Instituto de Microelectroínica de Barcelona (IMB-CNM, CSIC), 08193 Cerdanyola, Barcelona, Spain

ARTICLE INFO

Article history:
Received 24 February 2016
Received in revised form 8 April 2016
Accepted 19 May 2016
Available online 20 May 2016

Keywords:
Micromachined gas sensor
Nanowires
Electrodes
Optimization

ABSTRACT

Chemoresistive micromachined gas sensors with bottom-electrode configuration and based on Pt-functionalized tungsten oxide nanowires are fabricated. The performance and reliability of three types of devices with different electrode gap (5, 10 and 15 μm) are analyzed in dry and humid ambient and towards various analytes (H_2, NO_2, EtOH, and CO). Results demonstrate an improved response, sensitivity, and stability with better dynamic of the response for the sensors with the electrode gap of 5 μm, showing up to 7-fold higher responses and 32-fold faster responses towards hydrogen compared to the sensors with the electrode gap of 10 or 15 μm. These results are connected with the increment of the density of nanowire junctions across the electrodes with 5 μm gap; separation that corresponds to half of the length of the wires used in this work.

1. Introduction

Nanowire-based devices (e.g., chemical sensors or field-effect transistors) have demonstrated improved performance compared to their counterparts based in thin films, but the emerging of these structures as building blocks of micro/nano devices has also set fundamental challenges for the assembly technologies and the integrated-circuits industry, often due to the incompatibilities between the nanowire production on large scale and the micro/nano-device fabrication methods [1]. These incompatiblity issues hinder the use of certain technologies, for instance those utilized for fabricating Micro-Electro-Mechanical Systems (MEMS), which (among other ends) are commonly employed in chemoresistive gas sensors to reduce the electrical power consumption [2].

In chemoresistive nanowire-based gas sensors, nanowires bridge positive and negative electrodes to allow the electrical current to flow, and thus monitor the resistance or conductance changes produced by the adsorption of gaseous analytes at the surface of nanowires (typically metal oxides, although other materials such as silicon or carbon nanotubes CNTs are also used with the same principle) [1,3,4]. Consequently, the performance (particularly, response magnitude, sensitivity, stability, and reproducibility) of the gas sensor systems can be influenced by the features of both the electrodes and the sensitive material. Technologically, bottom-electrode architectures are preferred for chemoresistive nanowire-based sensors, as these systems do not require of post-processing steps for their integration, something that prevents the introduction of contaminants into the sensitive materials [3,5], whereas composite materials (e.g., nanowires functionalized with second-phase nanoparticles (NPs)) are preferred as sensitive materials due to their proved better gas sensing properties, originated from chemical and/or electronic sensitization mechanisms [6–8], particularly when the size of these materials is within the Debye length (L_D) of the surface (typically on the order of 2–100 nm) and the second-phase constituents are introduced in small, discrete amounts [8].

Nanowire assembly technologies generally include the transfer of pre-grown nanowires or the direct growth of nanowires onto the device. The first is largely used to integrate and align nanowires on the electrodes, though has proved critical in chemical sensing applications (e.g., gas sensing) due to the need of transfer media (e.g, liquids) that often degrade the surface properties of the wires [1]. The second, in contrast, avoids the use of transfer media and can simplify the processing steps for assembling nanowires, particularly when using bottom-up approaches (i.e., methods based on the growth of the structure through assemble of atoms derived from chemical precursors) rather than top-down approaches (i.e., methods based on carving, slicing or etching a macroscale material source) [9]. Chemical Vapor Deposition (CVD) and modifications such as Aerosol Assisted (AA) CVD are bottom-up techniques and

* Corresponding author.
E-mail address: vargas@feec.vutbr.cz (S. Vallejos).

http://dx.doi.org/10.1016/j.snb.2016.05.102
0925-4005/

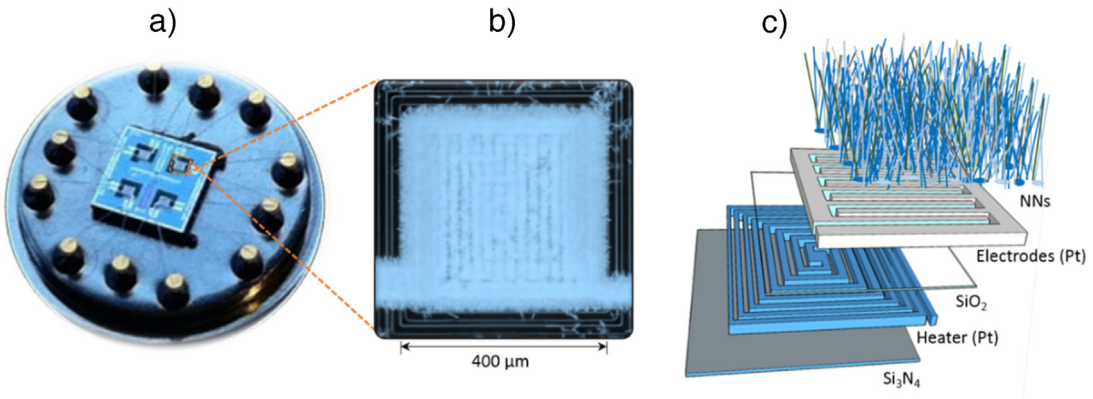

Fig. 1. Array of micromachined sensors mounted on a standard TO8 package (a), optical microscope imaging of the functionalized nanostructures grown directly on the micromachined platforms (b), and schematic view of the layers comprising the micromachined membrane (c).

have proved to be suitable for large-scale synthesis of nanowires both via vapor-liquid-solid (VLS) or vapor-solid (VS) mechanisms, i.e., with (for VLS) or without (for VS) the assistance of catalysts as seeds. [10]

Recently, we have developed a method for fabricating gas microsensors based on direct integration of nanowires into micromachined platforms and their functionalization with second-phase NPs in a single-step process via AA-CVD [11–13]. Those systems, based on bottom-electrodes and tungsten oxide nanowires, demonstrated improved sensing response compared to polycrystalline gas-sensitive films, as well as enhanced responses with faster response rates when the nanowires were functionalized with metals (e.g., Au, Pt) [11] or other metal oxides (e.g., Cu_2O [13], Fe_2O_3 [12]). However, despite having established the methods for processing these gas sensitive materials, the evaluation of the electrode configuration and its influence on the functionality of the whole sensor system has not been reported previously.

Here, we evaluate the performance and reliability of micromachined sensors, provided with different bottom interdigitated electrode (IDE) configuration, using Pt-functionalized tungsten oxide nanowires grown via AA-CVD as the sensitive material model. These microsensors are tested towards various gaseous species (H_2, NO_2, EtOH, and CO) in dry and humid ambient, and key factors of the sensor operation such as sensitivity, selectivity and stability are examined.

2. Experimental

2.1. Fabrication and processing steps

Micromachined platforms consisting of a suspended membrane (1 × 1 mm) of Si_3N_4 (300 nm thick), containing a Ti/Pt resistive heater (covering an area of 400 × 400 µm, 25 nm/250 nm thick, meander shaped) and Ti/Pt IDEs with different electrode gaps of 5, 10 or 15 µm (covering an area of 280 × 280 µm, 25 nm/250 nm thick), isolated by an interlevel silicon oxide layer (500 nm thick), were produced at wafer-level employing various microfabrication steps such as implantation, photolithography, etching, metallization, lift-off and rear side anisotropic etching of the substrate to define the membranes.

Pt-functionalized tungsten oxide nanowires were grown at 390 °C on the top of the electrodes via AA-CVD of tungsten hexacarbonyl (20 mg, $W(CO)_6$, Sigma-Aldrich, ≥97%) and hexachloroplatinic acid hydrate (4 mg, $H_2PtCl_6{\cdot}xH_2O$, Sigma-Aldrich,

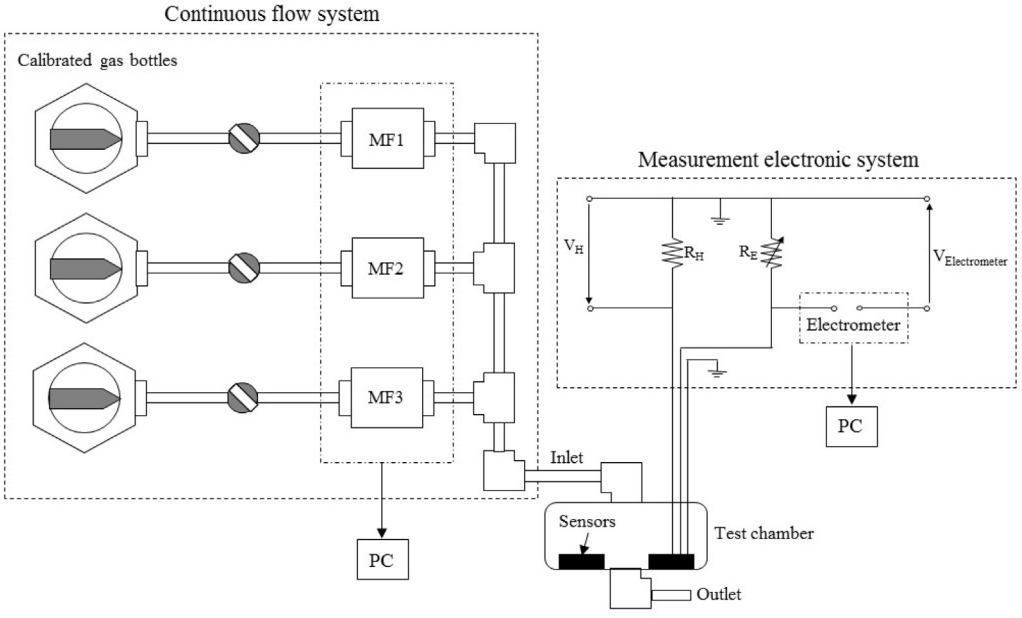

Fig. 2. Gas testing system. MF: mass flow, V_H: microheater bias voltage, R_H: microheater resistance, R_E: resistance of the gas-sensitive film (nanowires).

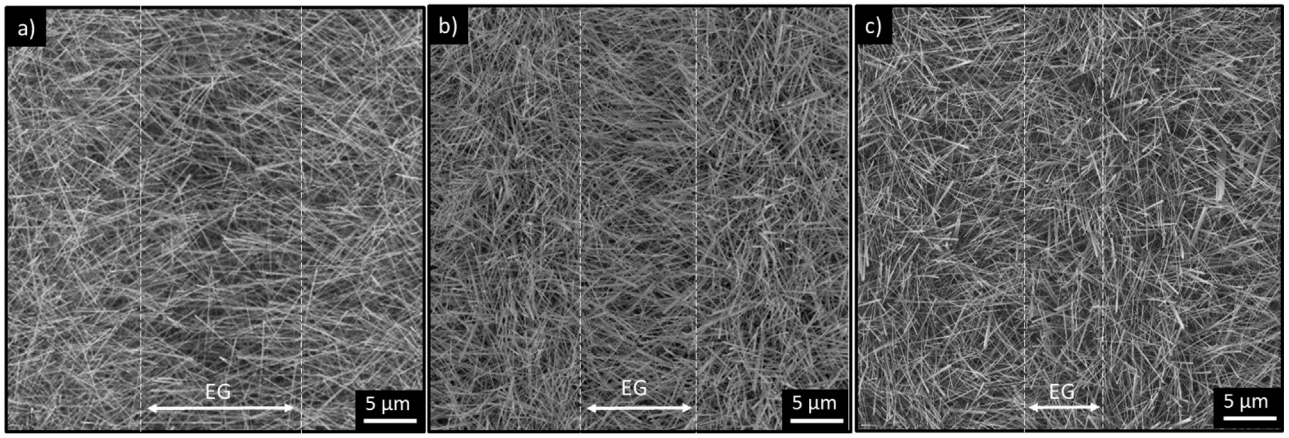

Fig. 3. SEM imaging (top view) of the functionalized nanowires integrated into the micromachined platforms with different IDE configuration. EG: 15 µm (a), EG: 10 µm (b) and EG: 5 µm (c).

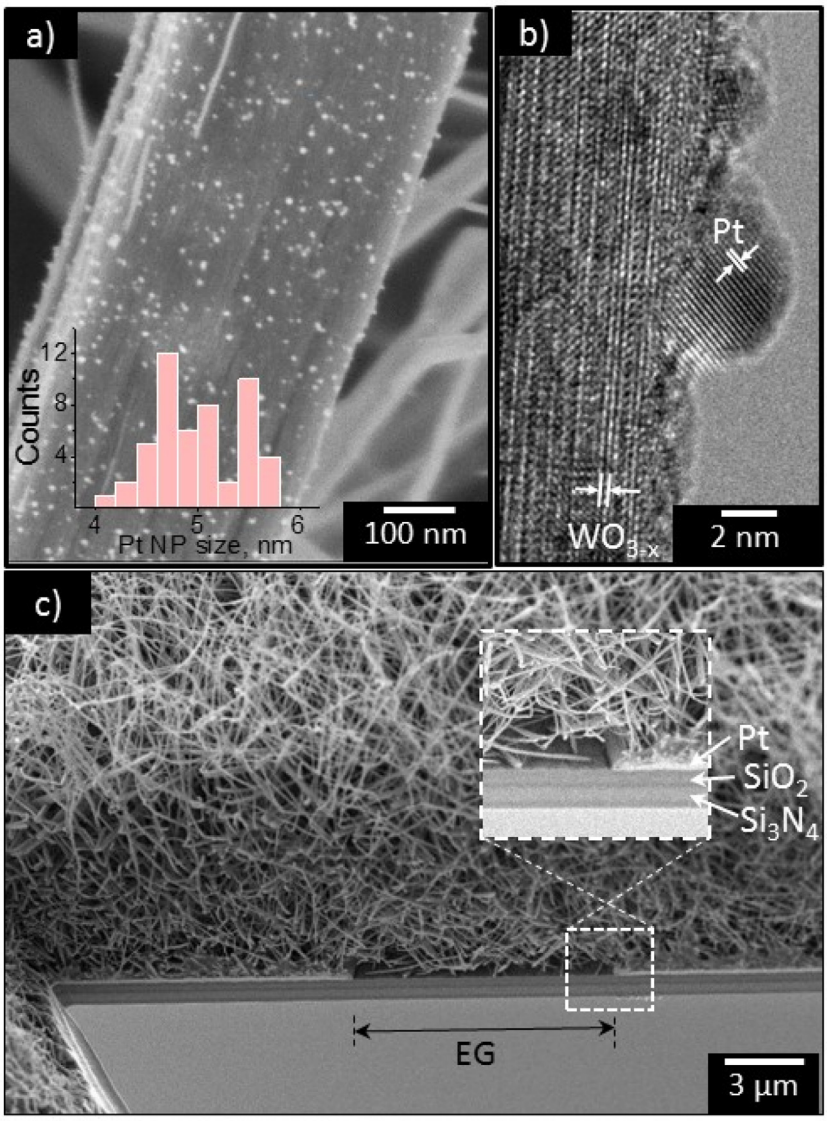

Fig. 4. High magnification SEM imaging of the functionalized nanowires grown on the micromachined platforms (a) and HRTEM of a single nanowire showing the planar distance for tungsten oxide and platinum (b). Cross-sectional SEM imaging of the micromachined sensors cut using FIB (c). Insets in (a) and (c) display the size of the platinum NPs dispersed along the nanowires and the layers comprising the microsensor, respectively.

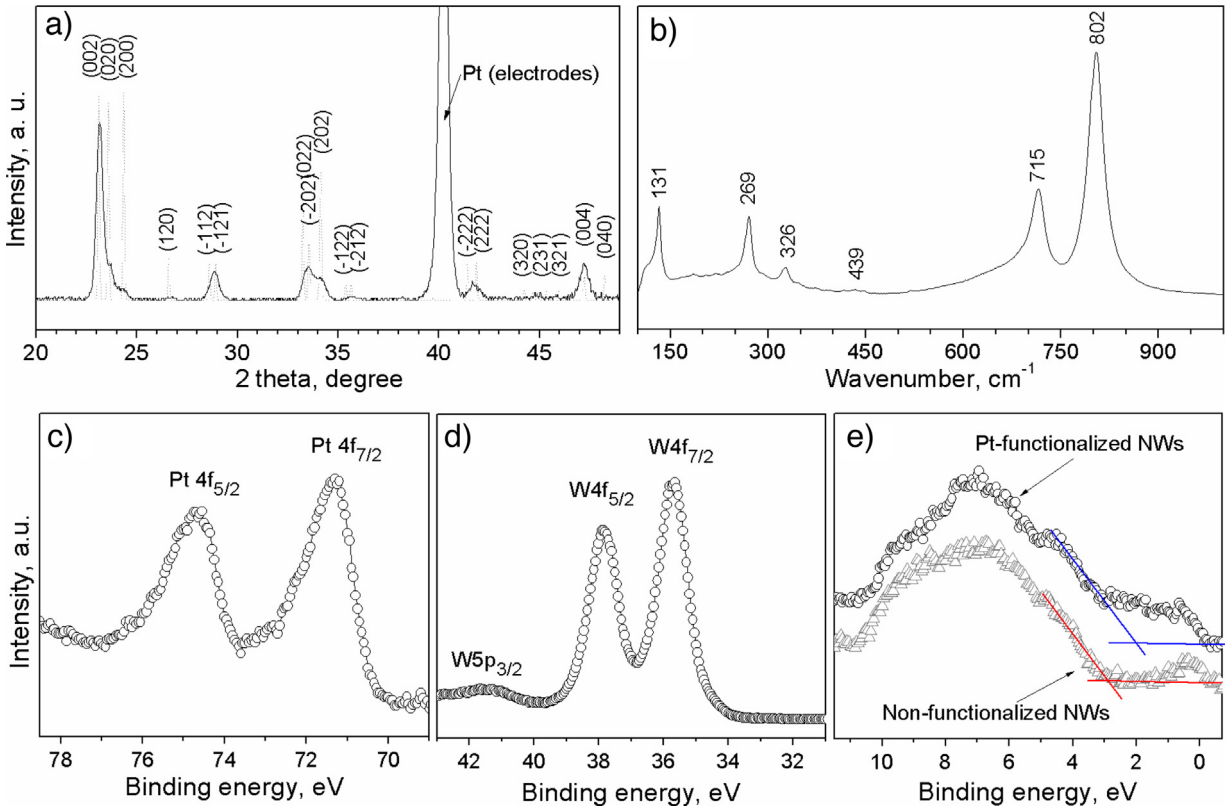

Fig. 5. XRD pattern (a), Raman spectra (b), and XPS spectra of the Pt 4f (c), W 4f core levels (d) and valence band (e) recorded on the Pt-functionalized nanowires. The valence band XPS spectra of similar non-functionalized nanowires grown via AA-CVD is included in (e) for reference.

99.9%) dissolved in methanol (5 ml, Sigma-Aldrich, ≥99.6%), as described previously [12]. A shadow mask was used during the deposition process, in order to protect the contacts and confine the film deposition to the electrode area. AA-CVD deposition was carry out simultaneously on various micromachined platforms with different electrode gaps to ensure relative similar characteristics of the sensitive material. After deposition, each chip containing an array of four microsensors was bounded and mounted on a standard TO-8 package (Fig. 1a). Fig. 1b shows a top view of the sensing active area of a sensor and Fig. 1c depicts the layers comprising the device.

2.2. Device characterization

The morphology of the films were examined using Scanning Electron Microscopy (SEM— Carl Zeiss, Auriga Series) and High Resolution Transmission Electron Microscopy (HRTEM — FEI Tecnai F20, 200 kV). Cross-section of the micromachined sensor was achieved by cutting the membrane with Focused Ion Beam (FIB — Carl Zeiss, 1560XB Cross Beam, 30 kV:200 pA). Moreover, the films were examined using X-ray Diffraction (XRD — Bruker, AXS D8-Advance, Cu Kα radiation operated at 40 kV and 40 mA), RAMAN (Renishaw in Via, laser of 514 nm, ion argon — Novatech, 25 mW) and X-ray photoelectron spectroscopy (XPS — Phoibos 150 analyzer — SPECS GmbH, Berlin, Germany — in ultrahigh vacuum conditions (base pressure 1×10^{-10} mbar) and a monochromatic Kα X-ray source, 1486.74 eV).

2.3. Gas sensing tests

Gas sensing tests were carried out towards various analytes by monitoring the electrical resistance changes of the films between room temperature (RT) and 350 °C and using a multimeter (Digital Multimeter Data Acquisition — Keithely 2700) configured with 20-channels relay multiplexer. The sensors were exposed to each analyte for 10 min in a continuous flow (200 sccm) test chamber (280 cm^3) with synthetic air as carrier gas (3X, Praxair). Subsequently, the chamber was purged with synthetic air during 30 min until the initial baseline resistance was recovered. Humidity was introduced to the system by bubbling through water under controlled conditions. To have a proper control of the relative humidity (RH) inside the gas test chamber an evaluation kit (EK-H4, Sensirion AG) with a humidity sensor (SHT71, operating ranges from 0 to 100% RH, accuracy of ±3% RH) was used. The total flow and exposition time for the humidity tests remained the same than those used for the gas testing in dry synthetic air. The sensor response (R) was defined as $R = R_a/R_g$ for reducing gases or $R = R_g/R_a$ for oxidizing gases, where R_a represents the sensor resistance in synthetic air at stationary state and R_g is the sensor resistance after 10 min of gas exposure. Calibrated cylinders of hydrogen (H_2, Praxair, 100 ppm), ethanol (EtOH, Praxair, 100 ppm) carbon monoxide (CO, Praxair, 100 ppm), and nitrogen dioxide (NO_2, Praxair, 100 ppm) diluted in synthetic air were further mixed with the carrier gas to obtain the desired concentration (Fig. 2). The gas testing results shown in Section 3 were recorded using various sensors with each electrode configuration for each testing condition (i.e., analyte, concentration, temperature, and relative humidity). The whole testing period spanned for the sensors was 140 days during which the same sensors were alternatively tested to the analytes at different concentrations and operating temperatures. Each measurement was replicated five times and during this test period, the array of sensors accumulated a total of 900 h of operation.

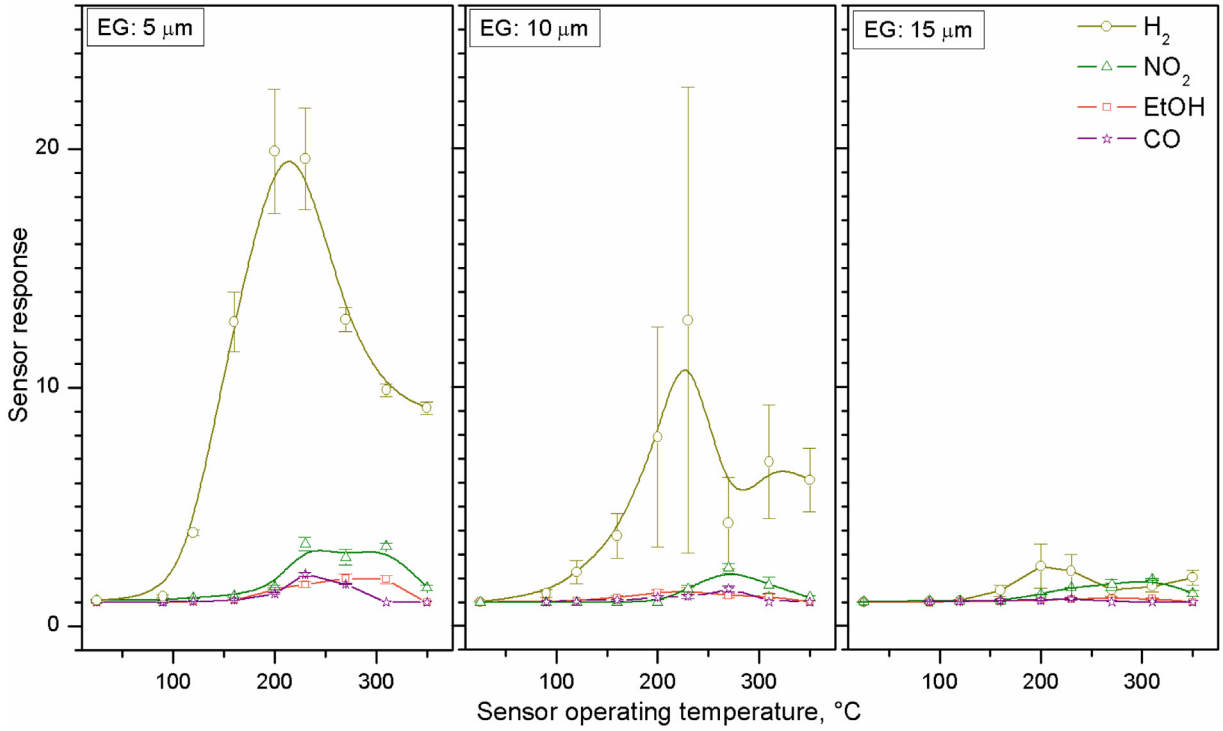

Fig. 6. Sensor response to 100 ppm of H_2, NO_2, EtOH and CO, displaying the mean and error bars of the measurements.

3. Results

3.1. Gas-sensitive material

Generally the properties of the sensitive films integrated into the micromachined platforms, with three different IDE configurations (identified as EG: 15, EG: 10 and EG: 5 μm), were in agreement with those observed in our previous work related to the functionalization of tungsten oxide nanowires with platinum NPs via AA-CVD [12]. SEM of the devices showed the films were deposited uniformly on the micromachined platforms, forming a mat-like network of non-aligned tungsten oxide nanowires interconnected across the IDEs (Fig. 3).

Further SEM of the nanowires, using in-lens detector, revealed the presence of NPs with 4–6 nm in diameter at the surface of the wire (Fig. 4a). Similarly, HRTEM (Fig. 4b) showed the presence of dispersed NPs at the surface with planar spacing of 2.21 Å (consistent with the internal lattice of the (111) plane of face-centered cubic Pt (d = 2.265 Å, ICCD card no. 04–0802)), and marked planar spacing of 3.55 Å along the nanowire (consistent with the monoclinic tungsten oxide phase identified by XRD (Fig. 5a)). Both, SEM and HRTEM showed wires with diameters between 100 and 400 nm, these values are larger compared to similar nanowires deposited using the same conditions on polymeric foils (between 50 and 100 nm) [12], likely due to the difference in surface roughness of the substrate. The cross-sectional SEM image of the microsensors performed in an area without the meander heater is shown in Fig. 4c; from bottom to top, it is observed the Si_3N_4 membrane, the interlevel SiO_2, the platinum electrode, and the nanowires with lengths of approximately 10 μm (due to the use of FIB for sectioning the device, the wires were damaged and the morphology appears degraded). Figs. 3 and 4 c also suggest a preference of the wires to grow on the electrodes, rather than in the gaps between electrodes, despite the fact that we proved previously the growth of these networked nanowires using similar AA-CVD conditions (without catalyst seeds) on various types of substrates (e.g., ceramic [14], polyimide [12], Si/SiO_2 [15]). This is likely related to the difference in thermal conductivity of platinum (the electrode) and Si_3N_4/SiO_2 (the membrane) and the action of thermophoretic effects during the AA-CVD process.

XRD of the sensing active area of the sensors (Fig. 5a) showed diffraction patterns associated with a monoclinic phase WO_3 (P21/n space group, a = 7.306°A, b = 7.540°A, c = 7.692°A, and β = 90.88°; ICCD card no. 72-0677), indicating a preferred orientation in the [001] direction with intense diffraction peaks at 23.1° 2θ (d = 3.85 Å) and 47.2° 2θ (d = 1.92 Å) that correspond the (002) and (004) reflections of this monoclinic phase (a platinum diffraction peak at approximately 40° 2θ coming from the electrodes was also observed). Similarly, Raman analysis (Fig. 5b) displayed well-defined Raman bands at 269, 326, 715 and 802 cm^{-1}. These bands fall close to the wavenumbers of the four strongest modes of monoclinic tungsten oxide [12,16,17]. The bands at 269 and 326 cm^{-1} are assigned to bending modes of the bridging oxygen, whereas the bands at 715 and 802 cm^{-1} are assigned to the stretching modes. The weak bands at around 439 cm^{-1} and the lattice modes below 200 cm^{-1} are typical bands of the crystalline tungsten oxide. These results demonstrate that the nanowires integrated into the micromachined devices (i.e., EG: 15 μm, EG: 10 and EG: 5) are characterized by a monoclinic-phase WO_3. XPS of the nanowires displayed Pt and W 4f core level peaks (Fig. 5c and d) with similar characteristics to those observed previously for Pt and tungsten oxide [11]. These results indicated O/W ratio of 2.6 and the incorporation of 10.7 wt.% of Pt at the wires. Examination of the valence band (VB) recorded near the Fermi energy level suggested an increase in the density of electronic states near the Fermi level (evidenced by comparing the VB spectra recorded for similar nanowires without functionalization), which could be associated with a strong electronic interaction between the platinum NPs and the tungsten oxide nanowires.

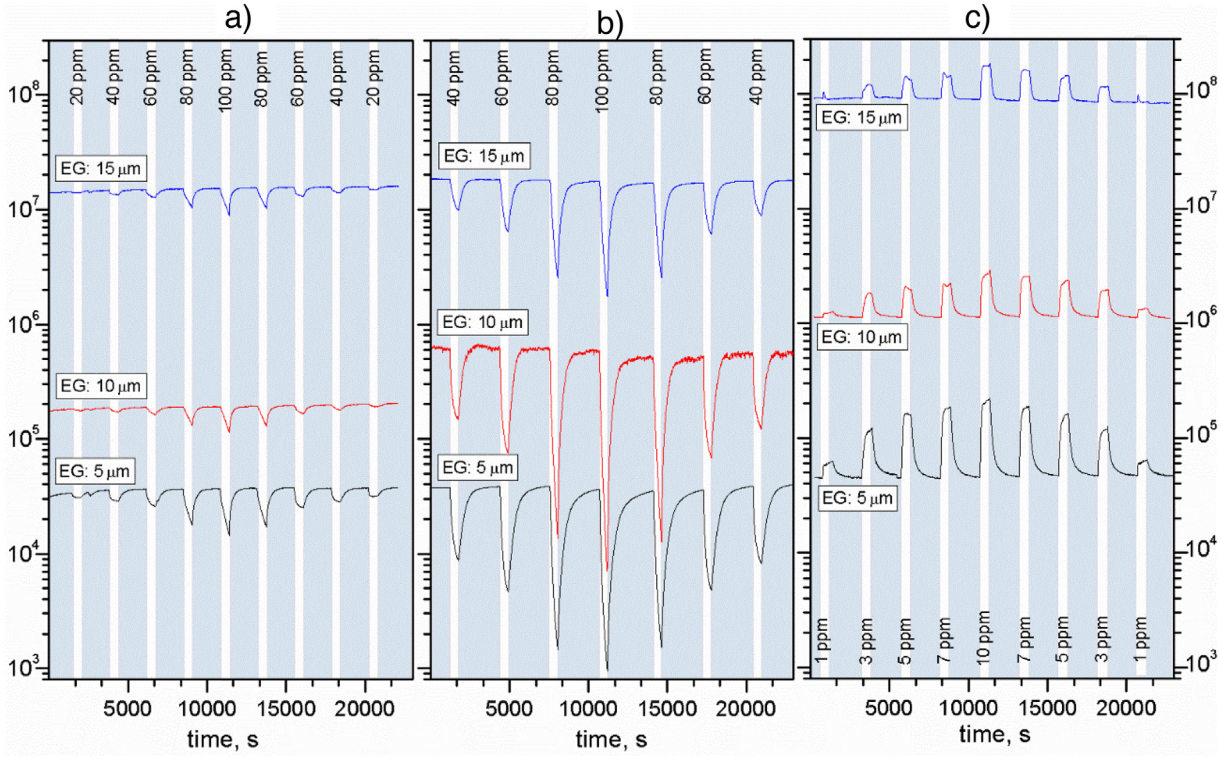

Fig. 7. Film-resistance changes towards EtOH (a), H_2 (b) and NO_2 (c) at 230 °C.

Table 1
Sensitivity of each sensors to EtOH, H_2 and NO_2 at 230 °C.

Sensor	Sensitivity (ΔR/ΔC)100%		
	EtOH $_{(20–100\,ppm)}$	$H_{2(40–100\,ppm)}$	$NO_{2(1–10\,ppm)}$
EG:5	1.6	37	39
EG:10	1.2	14	11
EG:15	0.8	11	1

3.2. Gas sensing tests

Tungsten oxide has been extensively studied for gas sensing application, demonstrating high sensitivity to various gaseous species, for instance in its intrinsic form to NO_2 [13,18–21] and O_3 [18,22], and when functionalized with platinum to H_2 [11]. In this work the devices were tested to NO_2, H_2, ethanol and CO at various sensor operating temperatures, between room temperature and 350 °C, using dc resistance measurements. The temperature dependency of the mean sensor response and standard error for each sensor and analyte at the same concentration is displayed in Fig. 6. Overall, results suggest a bell-shaped variation of the response and temperature with a maximum value between 200 and 240 °C and a marked high response to H_2, which shows a lower deviation (<12%) from the mean for the sensors with 5 μm of electrode gap, as opposed to the sensors with 10 μm (<70%) and 15 μm (<40 %) of electrode gap. This inverse relation between the response and the electrode gap is also noticed for the rest of analytes, with the change of electrical resistance to EtOH and CO becoming negligible for the electrodes with larger gap. For comparison, the responses to H_2 and NO_2 for the sensors with 5 μm of electrode gap were 7-fold and 1.5-fold higher, respectively, than those recorded on the sensors with 15 μm of electrode gap. Similarly, the response and recovery rates of the sensors with 5 μm of electrode gap were 32-fold and 14-fold faster, respectively, compared to those recorded for the sensors with 15 μm of electrode gap. This enhancement

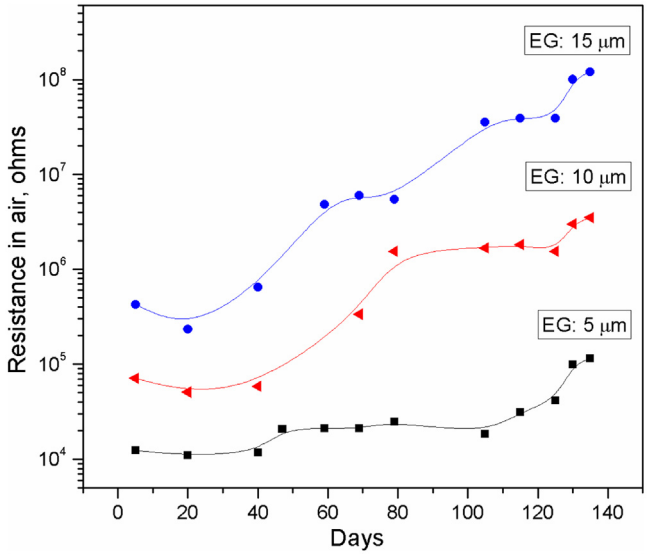

Fig. 8. Film-resistance in air for each type of sensors along 140 days of operation.

of the overall response in the sensors with 5 μm of electrode gap diminished the cross-response among the analytes and improved to some extent the discrimination of the analytes and the selectivity of the sensor device.

Fig. 7 shows a typical change of resistance to various analyte concentrations for each type of sensor. Responses displayed an *n*-type behavior to each analyte and a direct dependence of the response and gas concentration, indicating enhanced sensitivities (Table 1) for the sensors comprised of electrodes with narrower gaps (the sensitivity was defined in percentage as the ratio between the change in sensor response (ΔR) for a fixed change in analyte concentration (ΔC)).

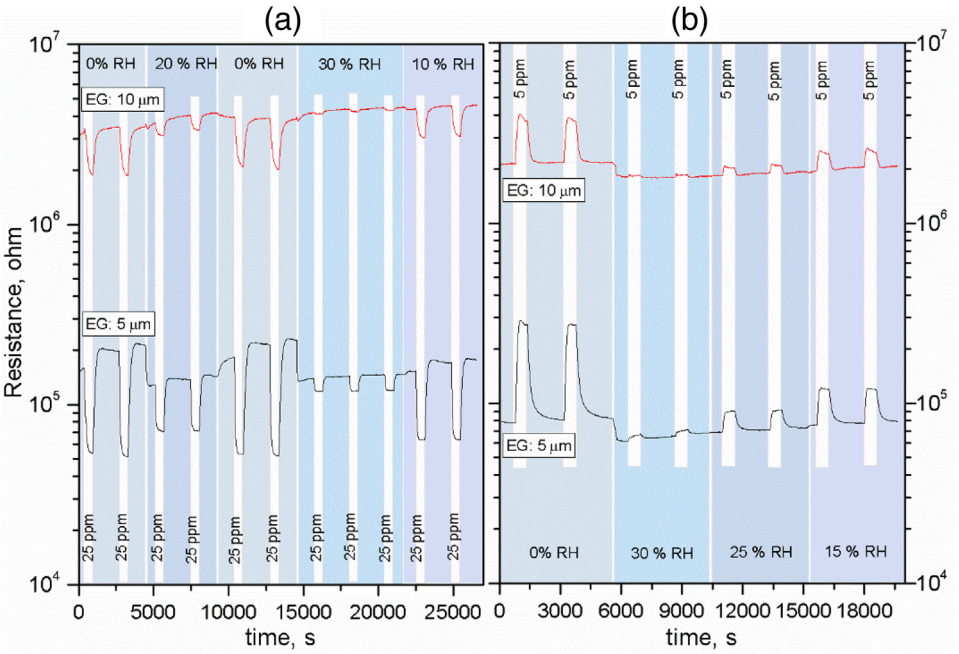

Fig. 9. Film-resistance changes towards dry and humid atmospheres in a background of synthetic air and H_2 (a) at 230 °C or NO_2 (b) at 270 °C.

Monitoring of the electrical resistance of the sensors in air along the testing period (140 days) showed drifts of the resistance with the lowest values measured during the first quarter of operation (e.g., 14 kΩ for EG: 5 μm, 90 kΩ for EG:10 μm, 200 kΩ for EG:15 μm at 230 °C) and the highest values in the last quarter (e.g., 100 kΩ for EG: 5 μm, 3 MΩ for EG: 10 μm, 110 MΩ for EG: 15 μm at 230 °C) (Fig. 8). These changes in the baseline resistance of the sensor were about 550-fold higher for the sensors with 15 μm of electrode gap compared to the sensors with 5 μm of electrode gap, which showed only 7-fold increase in resistance during the testing period.

After 120 days of operation (measuring the different analytes at various operating temperatures) the sensors with 15 μm of electrode gap lost response to analytes, thus the gas testing in humid ambient were carried out only for sensors with 5 and 10 μm of electrode gap. Test of the sensors in humid ambient to H_2 and NO_2 (Fig. 9) produced a decrease of the baseline resistance of the sensors (consistent with previous reports on Pt-functionalized tungsten oxide working in humid ambient) [23] and a drop-off the response to both analytes, which indicates a considerable influence of moisture in the behavior of the sensors. For instance at 30% RH the deviation of the sensor response relative to that measured in dry ambient to H_2 and NO_2 was higher (300%) for the sensors with 5 μm of electrode gap than for the sensors with 10 μm of electrode gap (70%).

3.3. Discussion

The characterization of the micromachined gas sensors based on functionalized nanowires and different bottom-electrode configurations showed enhanced performance (including higher responses and better sensitivities towards H_2, EtOH and NO_2, as well as better stability) for the systems comprised of electrodes with narrow gaps (i.e., sensors with IDEs separated by 5 μm). Similarly, results showed a boost in the resistance changes produced by the humidity when using the electrodes separated by 5 μm, and although this characteristic is not desirable in gas sensing, we noticed that the intrinsic sensitivity to humidity previously demonstrated on non-functionalized and Pt-functionalized tungsten oxide films [13,23,24] is also amplified by the use of the electrodes with narrow gap, analogously to that observed for H_2, EtOH and NO_2. The boost of response towards the gaseous analytes and humidity is linked with an optimization of the electrode gap relative to the length of the wires and an increment of the density of nanowire junctions (ρ) across the 5 μm electrode gap by 1.3 and 1.8 times compared to the sensors with 10 and 15 μm of electrode gap, respectively, (ρ = 438 for EG: 5 μm, ρ = 349 for EG: 10 μm, ρ = 241 for EG: 15 μm). These values (i.e., ρ) were estimated according to the expression reported previously for similar nanowire-based sensor assembly (non-micromachined) based on tin oxide [25]. Interestingly, a comparison of the gas sensing results reported previously for the tin oxide system to NO_2 at 300 °C [25] and our results for the tungsten oxide system to H_2 at 230 °C revealed that an increment of ρ by 1.3 registered in both cases an increase of the response to the analytes by 1.5. It is worth noting, however, that the density of junctions estimated for our system do not take into account the micromachined membrane deflection, which during operation bends its central point downwards the silicon bulk due to the bias voltage applied to the microheaters (7 μm at 230 °C, measured by interferometric microscopy). Similar remarks on the membrane deflection in micromachined platforms were also reported previously. [26] The bending of the micromachined platform could be responsible of the electrical resistance increase recorded in the films along the testing period (Fig. 8), as each time the microheaters were powered, the nanowire-nanowire junctions were subjected to a mechanical stress that could have deteriorated the nanowire junctions. This operational characteristic could also be responsible of the large deviation registered on the sensor response, as well as of the loss of long-term stability, particularly in the sensors with 15 μm of electrode gap, which have higher probability of losing the contact between nanowires due to the largest ratio between nanowire length and electrode gap, and the wires forming junctions apparently only at the end of the wire (as evidence in Fig. 3a). The nanowire-nanowire junctions (Fig. 10a) along the film play an important role in the overall response of the device, as the gas sensing mechanism depends on the modulation of the potential barriers originated during oxygen adsorption/desorption at the interface of the nanowires. These potential barriers are larger during oxygen adsorption due to the large surface depletion at the wires (Fig. 10b),

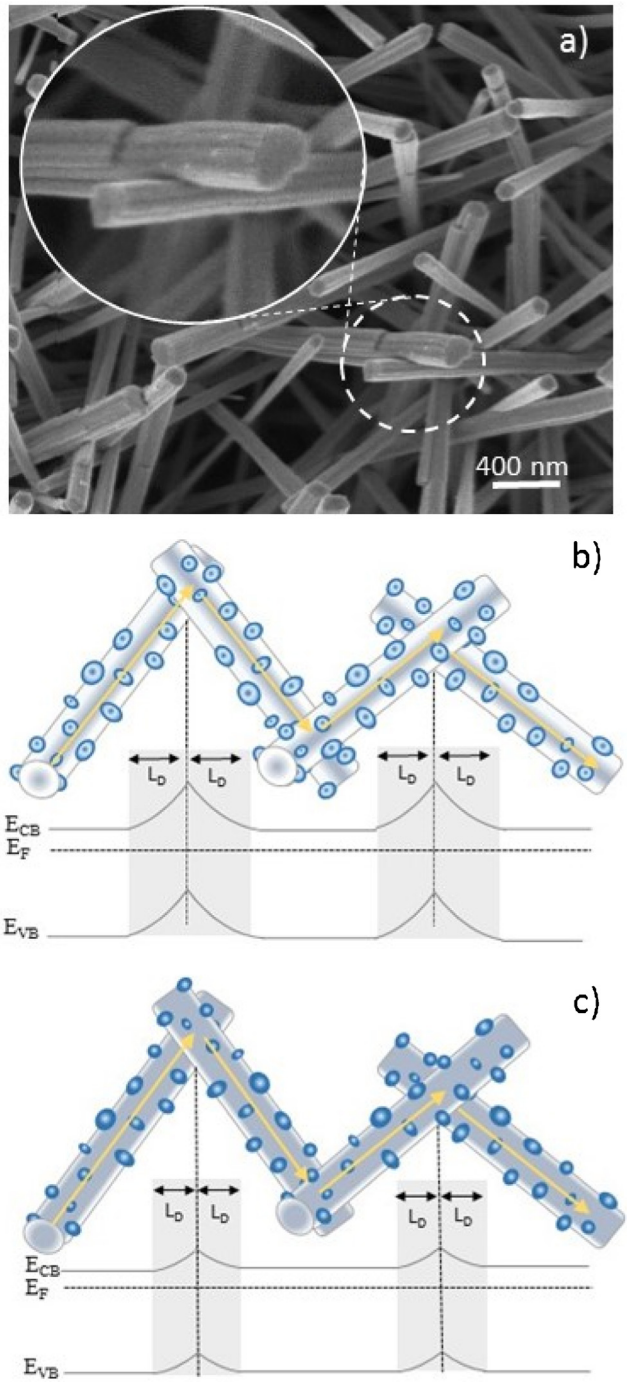

Fig. 10. SEM imaging of the junctions formed between functionalized nanowires (a) and schematic view of the interface gas sensing mechanism in networked nanowire films when exposed to air (b) and reductive analytes as hydrogen (c).

which increases the overall electrical resistance of the film. In contrast when the wires are exposed to reductive gases (e.g., H_2, EtOH, CO) the depletion layer along the wires and the potential barriers shrank (Fig. 10c), decreasing the electrical resistance of the film. It is worth noting that in present work the width of depletion at each wire and in turn the conduction channel along the wire are also influenced by the platinum NPs dispersed at the surface, as suggested by the intimate contact between these materials (Figs. 4 b and 5 e). Therefore the current flow in each nanowire is most likely tuned via two possible effects: spill over (i.e., the enrichment of the metal oxide surface with reactive species through catalysis) and/or Fermi level control (i.e., changes in the chemical state of the NPs with active species). The role of these mechanism in the enhancement of the sensing properties of the composite material were discussed previously [11].

Table 2 summarizes the sensing responses reported for various chemoresistive gas sensors based on Pt-functionalized tungsten oxide nanowires. Although comparison of sensor outputs is complex, as the overall sensor performance is influence by the sensing material features, the transducing platform employed and test parameters (operating temperature, flow, test cell volume), we consider these data is still meaningful to offer a general idea of the sensing properties observed for Pt-functionalized tungsten oxide nanowires and also the methods used for the integration of functionalized (decorated) nanowires into the sensor device. Overall, Table 2 shows Pt-functionalized tungsten oxide nanowires as sensing material for hydrogen, which is consistent with our results that also suggested a better affinity to this analyte (Fig. 6). It is also noticed, that the sensor responses registered in this work to H_2 are higher compared to our previous work on flexible platforms [12] in which a similar material processing method was used for the synthesis of Pt-functionalized tungsten oxide nanowires. These sensor responses are also higher than other works in the literature, with an exception of our study on Pt-functionalized tungsten oxide wires (second row in Table 2), which showed a relative higher response to H_2, likely due to the different characteristics of both the sensitive material and the micromachined platform; some of the relevant differences of the previous and present work include: 1) the utilization of $W(OPh)_6$ [11] instead of $W(CO)_6$, 2) the use of lower metal:tungsten ratio in the precursor solution and as consequence the result of lower Pt:W ratio in the film (found: 1% [11] instead of 15%), and 3) the use of lager micromachined membranes with the heaters covering 10 times more the area of the electrodes as opposed to the present system which has a relation of 2. An interesting point in Table 2, needed also to be emphasized, is that the CVD methods allow for the direct integration of functionalized nanowires with advanced sensor platforms (e.g., micromachined, flexible) in a single-step, providing an important process benefit compared to other competing synthetic techniques.

In summary, results showed improved performance and reliability for the sensors with IDEs separated by 5 μm, as opposed to those with IDEs separated by 10 or 15 μm, demonstrating the influence of the electrode features in the performance of chemoresistive gas sensors based on functionalized nanowires.

4. Conclusions

Micromachined gas sensors comprising different bottom-electrode configurations (EG: 5, 10 and 15 μm) and based on Pt-functionalized tungsten oxide nanowires integrated directly via AA-CVD were fabricated. Gas testing of these devices to various analytes (H_2, NO_2, EtOH, and CO) in dry and humid environment showed improved response, sensitivity and stability, with better dynamic of the response towards H_2 for the sensors based on electrodes with narrow gaps (i.e., 5 μm). These results showed up to 7-fold higher responses and 32-fold faster responses and relative better stability compared to the sensors with 10 and 15 μm of electrode gap. Results were attributed to the increment of the density of nanowire junctions across the electrodes with narrow gap. These junctions improve not only the conduction channel of the networked wires, but also increase the potential barriers which play an important role in the gas sensing mechanism of the whole film. Overall, these results suggest that to optimize the performance and reliability of chemoresistive nanowire-based gas sensors with bottom-electrode configuration, the gap between electrodes should be at least half the length of the wires.

Table 2
Summary the sensing responses reported for chemoresisitve gas sensors based on Pt-functionalized tungsten oxide nanowires. Selected parameters such as the characteristics of the materials, synthesis method, sensor technology and test conditions are pointed out.

Morphology	Features, nm	Method	Sensor platform	Electrode type	T_{op}°C	Gas	C ppm	R_a/R_g	Ref.
NPs@NWs	$(4–6)^{ØP}$ $(100–400)^{ØW}$ – 10000^{LW}	CVD^{Direct}	Si–μM	Bottom $IDEs^{5\,\mu m}$	200	H_2 NO_2	100	20	This work
							10	2.6	
NPs@NWs	$(1–4)^{ØP}$ $(60–120)^{ØW}$ – 7000^{LW}	CVD^{Direct}	Si–μM	Bottom $IDEs^{50\,\mu m}$	220	H_2	100	27	[11]
NPs@NWs	$(1–5)^{ØP}$ $(50–100)^{ØW}$ – 10000^{LW}	CVD^{Direct}	Flex	Bottom $IDEs^{5\,\mu m}$	250	H_2	100	6.25	[12]
NPs@NWs	$(30–200)^{ØP}$ $100^{ØW}$ – 10000^{LW}	$TE + SPT^{Transfer}$	Si	Top $IDEs^{20\,\mu m}$	300	CO NO_2	30	1.05	[27]
							10	1.03	
NPs@NWs	$(30–200)^{ØP}$ $50^{ØW}$ – 2000^{LW}	$TE + SPT^{Direct}$	Ceramic	Bottom $IDEs^{200\,\mu m}$	200	H_2	1000	1.53	[28]
NPs@NWs	$(3–5)^{ØP}$ $50^{ØW}$ – 2000^{LW}	$E + SPT^{Direct}$	Ceramic	Bottom $IDEs^{50\,\mu m}$	RT	H_2	1000	1.82	[29]
NPs@NWs	$(4–7)^{ØP}$ $370^{ØW}$	$ES + WCS^{Transfer}$	Ceramic	Bottom	350	C_3H_6O	5	8.50	[30]

NPs: nanoparticles, NWs: nanowires, ØP: diameter of the particles, ØW: diameter of the wires, LW: length of the wires, CVD: chemical vapour deposition, TE: thermal evaporation, E: evaporation of metallic tungsten, ES: electrospinning, SPT: sputtering, WCS: wet-chemical solution, Si–μM: silicon based micromachined platform, Flex: polymeric-based platform, IDEs: interdigitated electrodes.

Acknowledgments

This work has been supported, in part, by the SoMoPro II Programme, cofinanced by the European Union and the South-Moravian Region, via Grant 4SGA8678, and the Spanish Ministry of Science and Innovation via Grant TEC-2013-48147. O.Ch. is supported by project FEKT-S-14-2300 “A new types of electronic circuits and sensors for specific applications”. Part of this research has used the infrastructures of the SIX Research Centre.

References

[1] Y. Li, J.-J. Delaunay, *Nanowires*, in: P. Prete (Ed.), InTech, 2010.
[2] S. Sharma, M. Madou, A new approach to gas sensing with nanotechnology, Phil. Trans. R. Soc. Lond. A Math. Phys. Eng. Sci. 370 (2012) 2448–2473.
[3] A. Cao, E. Sudhölter, L. de Smet, Silicon nanowire-based devices for gas-phase sensing, Sensors 14 (2013) 245.
[4] Y. Wang, J.T.W. Yeow, A review of carbon nanotubes-based gas sensors, J. Sens. 2009 (2009) 24.
[5] S.-H. Jung, S.-W. Choi, S.S. Kim, Fabrication and properties of trench-structured networked SnO_2 nanowire gas sensors, Sens. Actuators B 171–172 (2012) 672–678.
[6] N. Yamazoe, G. Sakai, K. Shimanoe, Oxide semiconductor gas sensors, Catal. Surv. Asia 7 (2003) 63–75.
[7] X. Yang, V. Salles, Y.V. Kaneti, M. Liu, M. Maillard, C. Journet, X. Jiang, A. Brioude, Fabrication of highly sensitive gas sensor based on Au functionalized WO3 composite nanofibers by electrospinning, Sens. Actuators B Chem. 220 (2015) 1112–1119.
[8] D.R. Miller, S.A. Akbar, P.A. Morris, Nanoscale metal oxide-Based heterojunctions for gas sensing: a review, Sens. Actuators B 204 (2014) 250–272.
[9] E. Comini, C. Baratto, G. Faglia, M. Ferroni, A. Vomiero, G. Sberveglieri, Quasi-one dimensional metal oxide semiconductors: preparation, characterization and application as chemical sensors, Prog. Mater Sci. 54 (2009) 1–67.
[10] S. Vallejos, F. Di Maggio, T. Shujah, C. Blackman, Chemical vapour deposition of gas sensitive metal oxides, Chemosensors 4 (2016) 4.
[11] S. Vallejos, P. Umek, T. Stoycheva, F. Annanouch, E. Llobet, X. Correig, P. De Marco, C. Bittencourt, C. Blackman, Single-Step deposition of Au- and Pt-nanoparticle-functionalized tungsten oxide nanoneedles synthesized via aerosol-assisted CVD, and used for fabrication of selective gas microsensor arrays, Adv. Funct. Mater. 23 (2013) 1313–1322.
[12] S. Vallejos, I. Gràcia, E. Figueras, C. Cané, Nanoscale heterostructures based on Fe_2O_3@WO_{3-x} nanoneedles and their direct integration into flexible transducing platforms for toluene sensing, ACS Appl. Mater. Interface 7 (2015) 18638–18649.
[13] F.E. Annanouch, Z. Haddi, S. Vallejos, P. Umek, P. Guttmann, C. Bittencourt, E. Llobet, Aerosol-assisted CVD-grown WO_3 nanoneedles decorated with copper oxide nanoparticles for the selective and humidity-resilient detection of H_2S, ACS Appl. Mater. Interface 7 (2015) 6842–6851.
[14] S. Vallejos, T. Stoycheva, P. Umek, C. Navio, R. Snyders, C. Bittencourt, E. Llobet, C. Blackman, S. Moniz, X. Correig, Au nanoparticle-functionalised WO_3 nanoneedles and their application in high sensitivity gas sensor devices, Chem. Commun. 47 (2011) 565–567.
[15] S. Vallejos, P. Umek, C. Blackman, AACVD control parameters for selective deposition of tungsten oxide nanostrucutres, J. Nanosci. Nanotechnol. 11 (2011) 8214–8220.
[16] C. Santato, M. Odziemkowski, M. Ulmann, J. Augustynski, Crystallographically oriented mesoporous WO_3 films: synthesis, characterization, and applications, J. Am. Chem. Soc. 123 (2001) 10639–10649.
[17] J.Y. Luo, S.Z. Deng, Y.T. Tao, F.L. Zhao, L.F. Zhu, L. Gong, J. Chen, N.S. Xu, Evidence of localized water molecules and their role in the gasochromic effect of WO_3 nanowire films, J. Phys. Chem. C 113 (2009) 15877–15881.
[18] O. Berger, T. Hoffman, W.J. Fischer, V. Melev, Tungsten-oxide thin films as novel materials with high sensitivity and selectivity to NO_2, O_3, and H_2S. Part II. Application as gas sensors, J. Mater. Sci. Mater. Electron. 15 (2004) 483–493.
[19] J. Tamaki, T. Hashishin, Y. Uno, D.V. Dao, S. Sugiyama, Ultrahigh-sensitive WO_3 nanosensor with interdigitated Au nano-electrode for NO_2 detection, Sens. Actuators B 132 (2008) 234–238.
[20] C. Zhang, M. Debliquy, A. Boudiba, H. Liao, C. Coddet, Sensing properties of atmospheric plasma-sprayed WO_3 coating for sub-ppm NO2 detection, Sens. Actuators B 144 (2010) 280–288.
[21] M. Hu, J. Zeng, W. Wang, H. Chen, Y. Qin, Porous WO3 from anodized sputtered tungsten thin films for NO2 detection, Appl. Surf. Sci. 258 (2011) 1062–1068.
[22] S. Vallejos, V. Khatko, K. Aguir, K.A. Ngo, J. Calderer, I. Gràcia, C. Cané, E. Llobet, X. Correig, Ozone monitoring by micro-machined sensors with WO_3 sensing films, Sens. Actuators B 126 (2007) 573–578.
[23] C. Zhang, A.-F. Kanta, H. Yin, A. Boudiba, J. D'Haen, M.-G. Olivier, M. Debliquy, H_2 sensors based on WO_3 thin films activated by platinum nanoparticles synthesized by electroless process, Int. J. Hydrogen Energy 38 (2013) 2929–2935.
[24] W.-T. Koo, S.-J. Choi, N.-H. Kim, J.-S. Jang, I.-D. Kim, Catalyst-decorated hollow WO_3 nanotubes using layer-by-layer self-assembly on polymeric nanofiber templates and their application in exhaled breath sensor, Sens. Actuators B 223 (2016) 301–310.
[25] J.Y. Park, S.-W. Choi, S.S. Kim, Junction-tuned SnO_2 nanowires and their sensing properties, J. Phys. Chem. C 115 (2011) 12774–12781.
[26] J. Puigcorb, D. Vogel, B. Michel, A. Vil, I. Gracia, C. Cané, J.R. Morante, Thermal and mechanical analysis of micromachined gas sensors, J. Micromech. Microeng. 13 (2003) 548.
[27] S. Park, H. Kim, C. Jin, S.-W. Choi, S.S. Kim, C. Lee, Enhanced CO gas sensing properties of Pt-functionalized WO_3 nanorods, Thermochimica Acta 542 (2012) 69–73.
[28] L.F. Zhu, J.C. She, J.Y. Luo, S.Z. Deng, J. Chen, X.W. Ji, N.S. Xu, Self-heated hydrogen gas sensors based on Pt-coated $W_{18}O_{49}$ nanowire networks with high sensitivity, good selectivity and low power consumption, Sens. Actuator B 153 (2011) 354–360.
[29] L.F. Zhu, J.C. She, J.Y. Luo, S.Z. Deng, J. Chen, N.S. Xu, Study of physical and chemical processes of H_2 sensing of Pt-coated WO_3 nanowire films, J. Phys. Chem. C 114 (2010) 15504–15509.
[30] J. Shin, S.-J. Choi, D.-Y. Youn, I.-D. Kim, Exhaled VOCs sensing properties of WO_3 nanofibers functionalized by Pt and IrO_2 nanoparticles for diagnosis of diabetes and halitosis, J. Electroceram. 29 (2012) 106–116.

Biographies

S. Vallejos is currently SoMoPro --- Marie Curie fellow at Brno University of Technology. She received her Ph.D. degree from the Universitat Rovira i Virgili and has been working earlier at the Instituto de Microelectrónica de Barcelona and the University College London. Her current research is generally focused on gas sensing technologies and nanomaterials. She is interested in exploring scalable synthesis methods able to tailor and engineer the sensing properties of nanomaterials, as well as in the development of gas sensing microsystems for applications in safety, security and air quality monitoring.

I. Grácia received her Ph.D. degree in physics in 1993 from the Autonomous University of Barcelona, Spain, working on chemical sensors. She joined the National Microelectronics Center (CNM) working on photolithography, currently she is full time senior researcher in the Micro-Nano Systems department of the CNM and her work is focused on gas sensing technologies and MEMS reliability.

O. Chmela received his diploma in microelectronics in 2013 from the Brno University of Technology, Faculty of Electrical Engineering and Communications, Czech

Republic. Currently, he is PhD student at Brno University of Technology. His research is focused on fabrication of nanowire-based devices for sensing applications.

E. Figueras graduated in Physics in 1983 at Universitat Autonoma de Barcelona and received his Ph.D. Physics in 1988. Since 1989 is Tenured Scientist (Científico Titular) at the Microelectronic Institute of Barcelona (IMB-CNM. CSIC). He spent ten years as head of the clean room, carrying out the standardization of the new technologies developed at the Institute. Since 2000 his research is in the field of micro/nanostructures for gas sensors.

J.Hubálek received his Ph.D. degree in 2003 from Brno University of Technology. He works with micro- and nanotechnologies for sensing. He has experiences with gas sensors preparation and electrochemical sensors and instrumentation. He is group leader of Laboratory of Microsensors and nanotechnologies at SIX centre and group of Smart Nanodevices at CEITEC centre

C. Cané is Telecommunications Engineer and he received his Ph.D. in 1989. Since 1990 he is a full time senior researcher at CNM and has been working in the development of CMOS technologies and also on mechanical and chemical sensors and microsystems. He is member of the technical committee of EURIMUS-EUREKA programme since 1999. Over the years he has been coordinator of several R&D projects, both at national and international level in the MST field. He has performed management activities as head of the Microsystems and Silicon Technologies Department of CNM and as vice-director of CNM in Barcelona. He is the coordinator of the GoodFood Integrated Project from the 6th Framework Programme (FP6-IST-508774-IP).